Available online at www.sciencedirect.com

ScienceDirect

journal homepage: www.elsevier.com/locate/he

Two-controlling mechanisms model for hydrogen desorption in the $Li_4(NH_2)_3BH_4$ doped $Mg(NH_2)_2$–2LiH system

G. Amica [a,b,c], F. Cova [a,b,d,*], P. Arneodo Larochette [a,b,c], F.C. Gennari [a,b,c]

[a] Consejo Nacional de Investigaciones Científicas y Técnicas (CONICET), Av. Bustillo 9500, R8402AGP, S. C. de Bariloche, Río Negro, Argentina
[b] Centro Atómico Bariloche (CNEA), Av. Bustillo 9500, R8402AGP, S. C. de Bariloche, Río Negro, Argentina
[c] Instituto Balseiro, Universidad Nacional de Cuyo, Argentina
[d] Institut Néel, Centre National de la Recherche Scientifique (CNRS), 25 Avenue des Martyrs, 38042, Grenoble, France

ARTICLE INFO

Article history:
Received 21 September 2016
Received in revised form
10 November 2016
Accepted 10 November 2016
Available online 1 December 2016

Keywords:
Hydrogen storage
Amides
Kinetics
Controlling mechanism

ABSTRACT

The limiting step of the dehydrogenation process and the desorption kinetic model of the composite $0.7Mg(NH_2)_2$–$1.4LiH$–$0.2Li_4(NH_2)_3BH_4$ under different hydrogen back pressures at low temperature (200 °C) were studied in this work. It was determined that a single mechanism model was not able to explain the behavior of the reaction at low and high reacted fractions simultaneously. A combination of two controlling mechanisms, which reproduce accurately the behavior of the system, was proposed. The rate equation deduced involves the contribution of a second grade Avrami model and a 3D diffusion model as a function of pressure and conversion. At low conversions, the limiting step of the reaction is the formation of the products. Once a thin layer of product is formed on the surface, the diffusion through it becomes the new limiting step. With pressure increase, the mechanism change occurs later during desorption due to the higher difficulty in creating nucleation points on a surface exposed to a higher concentration of hydrogen.

Introduction

Solid-state hydrogen storage for mobile applications is a safe and efficient method which provides improved volumetric energy densities at moderate pressures and temperatures. Among the complex metal hydrides storage systems intensively explored in the past years, the $Mg(NH_2)_2$–LiH composite has attractive features for onboard utilization owing to its good reversibility, moderate operating temperatures, 5.5 wt% hydrogen content, and suitable ΔH (~44.1 kJ mol^{-1} H_2), determining a desorption temperature lower than 100 °C at atmospheric pressure [1–6]. The hydrogen sorption reaction was presented by Hu et al. [4], according to the following pathway:

$$2Mg(NH_2)_2 + 3LiH \rightarrow Li_2Mg_2(NH)_3 + LiNH_2 + 3H_2 \quad (1)$$

$$Li_2Mg_2(NH)_3 + LiNH_2 + LiH \rightarrow 2Li_2Mg(NH)_2 + H_2 \quad (2)$$

$$\text{In all: } 2Mg(NH_2)_2 + 4LiH \rightarrow 2Li_2Mg(NH)_2 + 4H_25.5\ \text{wt\%} \quad (3)$$

* *Corresponding author*. Institut Néel, Centre National de la Recherche Scientifique (CNRS), 25 Avenue des Martyrs, 38042, Grenoble, France.
E-mail address: federico.cova@neel.cnrs.fr (F. Cova).
http://dx.doi.org/10.1016/j.ijhydene.2016.11.079
0360-3199/

However, in order to achieve reasonable desorption rates, temperatures over 200 °C are required, indicating the presence of a relatively high kinetic barrier for this reaction to be surmounted, inhibiting its application as a commercial hydrogen storage material. One strategy in this direction, with positive effects on its kinetics, is the addition of catalysts, such as alkali metal compounds or metal borohydrides [7–13]. However, in order to improve the hydrogen desorption kinetics and lower the operating temperature, the reaction mechanism has to be understood. As it will be presented, a deep analysis of the kinetics of the Li–Mg–N–H system has not been conducted so far and there is no doubt that such complete studies are necessary in order to provide guidelines for improving the kinetics of this type of systems in the future.

The mechanism of the transformation between lithium amide and lithium imide for the Li–N–H system was proposed by David et al. [14]. They demonstrated that the rate controlling step was the movement of Li^+ in $LiNH_2$ to create a Frenkel defect pair, a charged interstitial $[LiLiNH2]^+$, and a lithium vacancy $[Li\square NH2]^-$ in a non-stoichiometric manner [14]. Wu et al. [15] found that in addition to the migration of the small mobile ions Li^+ and H^+, the mobile H^- in hydrides had a key role in the hydrogen storage of $Li_2Mg(NH)_2$. For the heterogeneous solid-state reaction of $Mg(NH_2)_2$ and LiH, Chen et al. [16] indicated that the reaction rate was controlled by the interface reaction between amide and hydride in the preliminary stage and mass transport through the imide layer in the subsequent stage. Then, the kinetics is particle size dependent. Concerned about the high operating temperature and slow kinetics that retarded the practical applications of the Li–Mg–N–H system, Liu et al. [6] investigated the dependence on particle size of the hydrogen storage performance. They synthesized $Li_2Mg(NH)_2$ by sintering a mixture of $Mg(NH_2)_2$–$2LiNH_2$ with a subsequent ball milling of the product for different periods to obtain particles of different sizes, and they observed that the particle size reduction improved sorption kinetic properties. For the dehydrogenation reaction, a three-dimensional diffusion-controlled kinetic mechanism was identified by analyzing isothermal hydrogen desorption curves. In agreement with previous works, it was concluded that the rate-controlling step for dehydrogenation of the Li–Mg–N–H system should be the diffusion of the mobile small ions in both the amide and the imide [6]. Markmaitree et al. studied the isothermal hydrogenating kinetics of the pure $Li_2Mg(NH)_2$ phase synthesized via dehydrogenating treatment of a ball milled $2LiNH_2$–MgH_2 mixture [17]. Even though different possible controlling mechanisms were taken into account, they concluded that the hydrogenation process of $Li_2Mg(NH)_2$ at 180, 200, and 220 °C could be described as a diffusion-controlled reaction [17]. A dependence of the onset dehydrogenation temperature and the dehydrogenation rates of the $Mg(NH_2)_2$–2LiH system on the gas back pressure was presented by Liang et al. [18]. It was found to be the key factor for the formation of different crystal structures of $Li_2Mg(NH)_2$ (cubic or orthorhombic). Considering all the information presented, it can be said that there seems to be a general agreement that there is a diffusion-controlled kinetic mechanism for both the Li–N–H and the Li–Mg–N–H systems [6,17,19,20].

Recent works have demonstrated that lithium fast-ion conductors have positive effects on the hydrogen storage properties of the Li–Mg–N–H system [12,13,21,22]. In our previous work, $Li_4(NH_2)_3BH_4$ doped $Mg(NH_2)_2$–2LiH was formed by mechanical milling of the $2LiNH_2$–MgH_2–$0.2LiBH_4$ mixture and posterior annealing under hydrogen pressure [23]. The ionic liquid $Li_4(NH_2)_3BH_4$ with low melting temperature showed a beneficial effect on the dehydrogenation behavior after successive cycles in comparison to the pristine material ($Mg(NH_2)_2$–2LiH). The dehydrogenation rate was doubled, while hydrogenation could be performed 20 times faster. Although the dehydrogenation rate decreased with the cycle number, the presence of $Li_4(NH_2)_3BH_4$ stabilized the hydrogen storage capacity with cycling. The catalytic role of $Li_4(NH_2)_3BH_4$ in improving the dehydrogenation kinetics was associated with the weakening of the N-H bond and the mobile small ion mass transfer enhancing.

The aim of this work is to determine, in the first instance, the limiting step during the dehydrogenation process of the composite $0.7Mg(NH_2)_2$–$1.4LiH$–$0.2Li_4(NH_2)_3BH_4$ under different hydrogen back pressures at low temperature (200 °C). Furthermore, it was attempted to model the desorption kinetics of the system taking into account the different models and equations proposed in the literature to predict the kinetics of metal-hydrogen systems. A single model was insufficient to describe adequately the kinetic performance of the doped composite in the complete range of the reaction at different hydrogen back pressures. The rate equation deduced involves the contribution of two models with different weights during the dehydrogenation process.

Experimental

Synthesis of the composites

The starting materials were commercial $LiNH_2$ (Aldrich, 95%), MgH_2 (Aldrich, 98%), and $LiBH_4$ (Aldrich, 90%). Due to the high reactivity of the samples, they were handled in an MBraunUnilab argon-filled glove box, with oxygen and moisture levels lower than 1 ppm. For all studies, high purity hydrogen (Linde, 99.999%) and argon (Linde, 99.999%) were used. The sample preparation was carried out by mechanical milling of the $2LiNH_2$–MgH_2–$0.2LiBH_4$ mixture, using a sequence of 15 min milling and 10 min pause in a planetary ball mill (Fritsch Pulverisette 6) at 500 rpm with a ball to powder mass ratio of 53:1. The sample was milled for 20 h and to eliminate possible dead zones, the material was manually mixed after 1 h, 3 h, 5 h, 10 h and 15 h. Then, the composite $0.7Mg(NH_2)_2$–$1.4LiH$–$0.2Li_4(NH_2)_3BH_4$ was obtained by this synthesis, followed by thermal treatment for 30 min at 200 °C under 6000 kPa of hydrogen [23]. It is worth pointing out the formation of the new phase $Li_4(NH_2)_3BH_4$ during mechanical milling and that no excess of any reactive was detected.

Characterization of the composites

Hydrogen storage properties of the sample were studied using modified Sieverts-type equipment, coupled with a mass flow controller. The sample was transferred in the glove box into a stainless steel reactor which was connected to the Sieverts device. Before the first dehydrogenation, the sample was

heated to the reaction temperature (200 °C) under hydrogen pressure of 6000 kPa and kept at this temperature for 30 min. As it was shown in our previous work [23], this pressure is more than enough to ensure that the sample does not dehydrogenate while heating. Dehydrogenation curves were obtained at a constant temperature of 200 °C. Different hydrogen back pressures (50, 450, 1000, 1500 and 2000 kPa) were employed to evaluate the effect of the pressure on the kinetics. These hydrogen back pressures were selected considering the equilibrium hydrogen pressure during dehydrogenation at 200 °C as 3000 kPa [23]. The rehydrogenation was performed at 200 °C with a constant hydrogen pressure of 6000 kPa. In order to obtain more reliable results, three measurements were performed at each back pressure using different samples every time, which allowed the introduction of error bars in the calculation of the principal parameters (x_0, K_1 and K_2). The amount of absorbed/desorbed hydrogen was determined with a relative error ±5%.

To determine the limiting step of the reaction during the dehydrogenation process and to find a model of the desorption kinetics of the system, different controlling mechanisms, such as nucleation, geometrical contraction, diffusion and reaction order were taken into account as a departing point and were then modified to consider pressure effects [24].

Computational details

The fitting of the desorption curves and the parameter determination was performed using a least squares method implemented in Matlab. In order to determine the parameters, a genetic algorithm was used to select a set of parameters for each iteration step [25]. This algorithm was successfully applied previously for the modeling of the Ni-catalyzed MgH_2 hydrogen absorption rate [26,27]. The total population for the algorithm was 200 sets of parameters and it was evolved until the convergence criterion was met. With these parameters, it was possible to simulate the desorption curve using the ode45 method provided by Matlab. The curve obtained was then compared to the experimental one and the goodness of the fitting was determined calculating the sum of the squared differences between the experimental and the calculated data. To advance into the next step of the iteration, the better fitting parameters were utilized to determine the new parameters. Each new generation was composed of: 25% of the most suitable sets from the previous generation, 25% of the sets generated by crossover from the previous ones, averaging all the parameters in the set, 25% of mutations obtained by the modification of one of the parameters in one of the selected sets by an order of magnitude, and 25% of immigrants generated randomly in the same way as the initial population. A difference smaller than 0.1% between the 25% best fitting sets of parameters within one generation was used as convergence criteria (an artificial minimum of 30 generations was imposed in order to prevent undesired early exits of the calculations).

Results and discussion

Hydrogen reaction kinetics of the samples were studied by continuous cycling in the Sieverts device at 200 °C with different back pressures (50–2000 kPa). The samples showed an absorption capacity between 4 and 4.5 wt% after several cycles of hydrogen absorption/desorption. Details about the hydrogen storage capacity and stability are presented elsewhere [23]. In our previous work, XRPD and FTIR analyses of the milled and cycled samples have been presented showing the phases present in the samples before and after the hydrogen cycling. The milled sample obtained was proved to be a mixture of $Mg(NH_2)_2$, $Li_4(NH_2)_3BH_4$ and LiH with a small amount of residual $LiNH_2$ and MgH_2. After submitting it to thermal treatment under hydrogen, neither $LiNH_2$, nor MgH_2, nor $LiBH_4$ were identified as unreacted phases. In the absorbed state, $Mg(NH_2)_2$, LiH and $Li_4(NH_2)_3BH_4$ were identified, and the presence of $Li_2Mg_2(NH)_3$ showed that the sample was partially rehydrogenated. For the dehydrogenated sample, only $Li_4(NH_2)_3BH_4$ and $Li_2Mg(NH)_2$ were identified, which evidenced the $Mg(NH_2)_2$ complete dehydrogenation [23]. Fig. 1 shows a

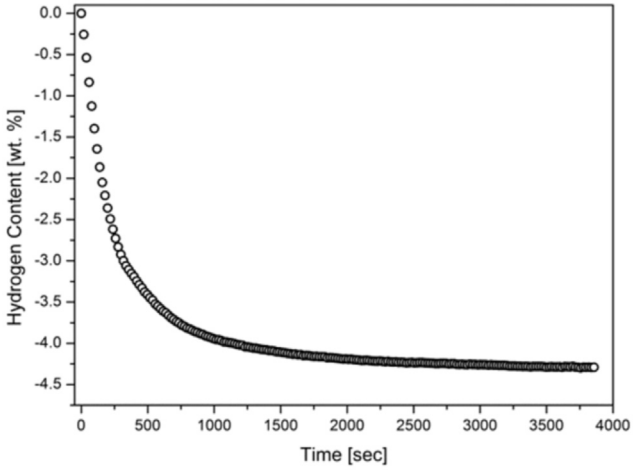

Fig. 1 – Second cycle of dehydrogenation at 200 °C of the ball milled sample with a back pressure of 50 kPa.

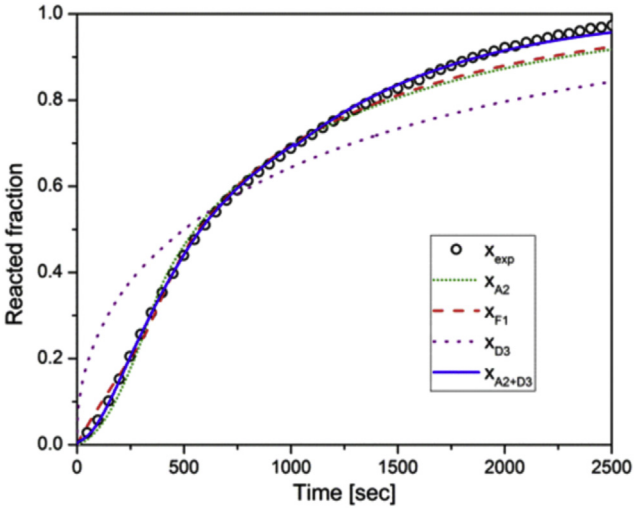

Fig. 2 – Desorption curve fitted with Avrami–Erofeev's nucleation model (A2), first order reaction model (F1), 3D diffusion model (D3) and a combination of two of them (A2 + D3).

typical desorption curve at 200 °C and 450 kPa of back pressure.

Several equations proposed in literature were considered to fit the data [28]. A complete summary of the different kinetic models, grouped in four subtypes according to the controlling mechanism: nucleation, geometrical contraction, diffusion and reaction order, has been presented [24]. Fig. 2 shows the comparison of a desorption curve fitted with three different single models, such as the Avrami–Erofeev's nucleation model (A2), the first order reaction model (F1), and the three-dimensional diffusion model (D3). It can be seen that none of the models were able to fit the experimental values at the beginning and at the end of the reaction simultaneously. In particular, the 3D diffusion model, which is agreed to be the controlling kinetic mechanism for Li–N–H systems, did not show good agreement. In order to overcome

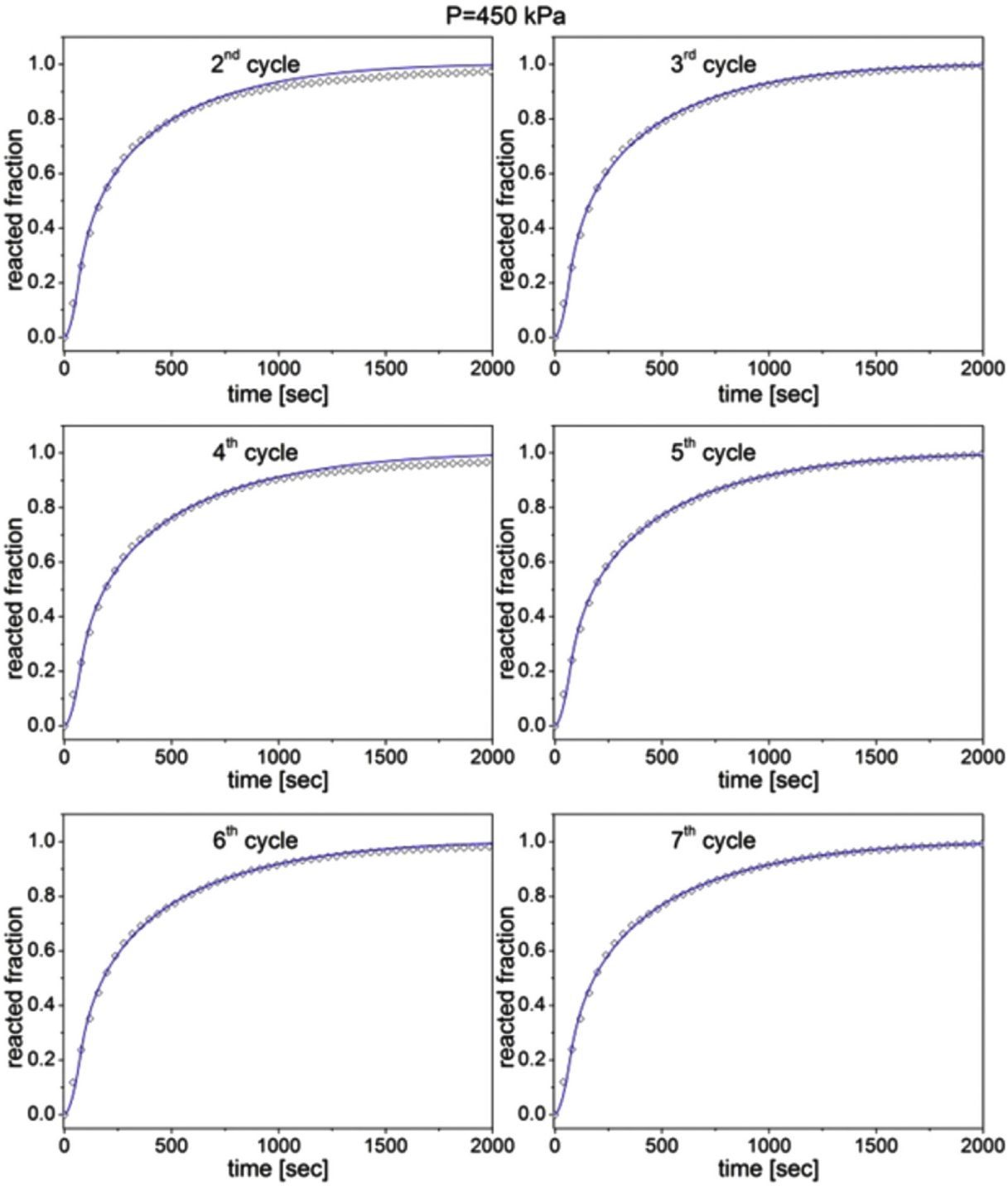

Fig. 3 – Curves calculated with the model combination A2 + D3 and the corresponding experimental data for different desorption cycles with a back pressure of 450 kPa.

this issue, a better approach could be reached by taking into account the contribution of two of the previously studied models, one that could fit the first stage and the other that could reproduce the behavior at higher conversions. A similar approach has been presented by Lozano et al. for sodium alanate [29].

Then, all the possible combinations between models were considered. A fitting algorithm which required the determination of the parameters K_1, K_2 (the kinetic constants for each model) and x_0 was prepared in order to determine the most adequate models. Physically, this can be considered as a change in the limiting step of the reaction during the dehydrogenation process. The general equation for the reaction rate using this approach is:

$$r = \alpha_1 r_1 + \alpha_2 r_2 \quad 01$$

where r_1 and r_2 are the reaction rates obtained using the expressions from the selected initial and final models, and α_1 and α_2 are the coefficients that weight the contribution of each model for a given conversion. For these factors, a step-like function was proposed; in particular, the logistic function was selected:

$$\alpha_1 = 1 - \frac{1}{1 + e^{-40(x - x_0)}} \quad 02A$$

$$\alpha_2 = 1 - \alpha_1 \quad 02B$$

where x_0 is the reacted fraction value at which the system changes from one controlling mechanism to the other. The reacted fraction x was defined as the ratio between the amount of hydrogen desorbed at a given time and the final amount of hydrogen released at the end of the reaction. The value 40 represents the steepness of the curve and was selected in order to ensure that the reaction transitioned from 90% of the first model to 90% of the second model, in a range of 0.1 for x. To obtain this value, the parameters were allowed to vary for all the measurements, and once obtained, the average value was selected, and then all the fittings were redone with this new value fixed.

The best fits were obtained using a second grade Avrami–Erofeev's model as the initial controlling mechanism and a 3D diffusion model as the final controlling mechanism.

Fig. 3 shows the curves calculated with the combined model and the corresponding experimental data for several desorption cycles. The first desorption is omitted because the system presented a different behavior in the initial desorption compared to the following cycles. This phenomenon is usual in $Mg(NH_2)_2$ based systems [23].

The combined model was also used to fit the desorption curves in a range of pressures between 50 kPa and 2000 kPa.

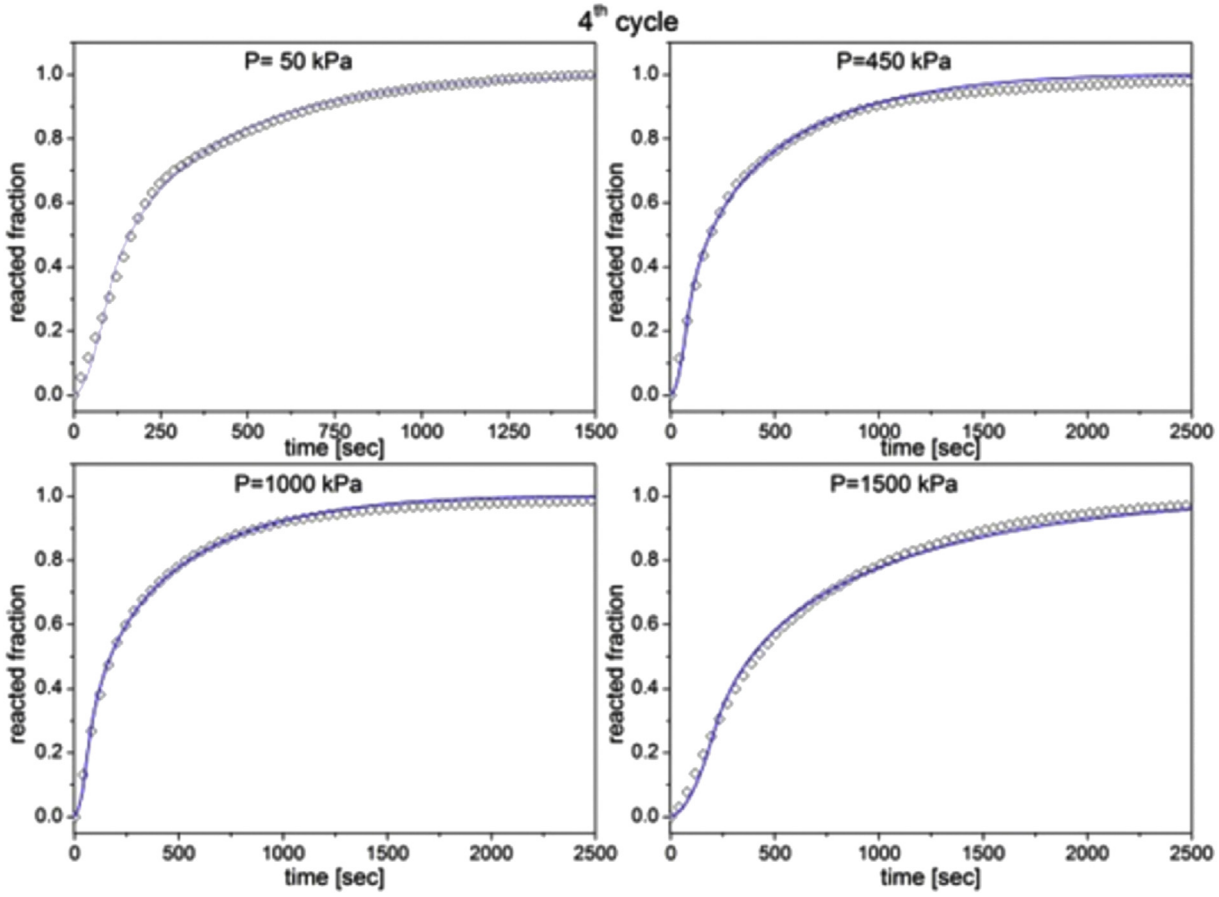

Fig. 4 – Curves calculated with the model combination A2 + D3 and the corresponding experimental data with different hydrogen back pressures (50, 450, 1000 and 1500 kPa) for the 4th cycle.

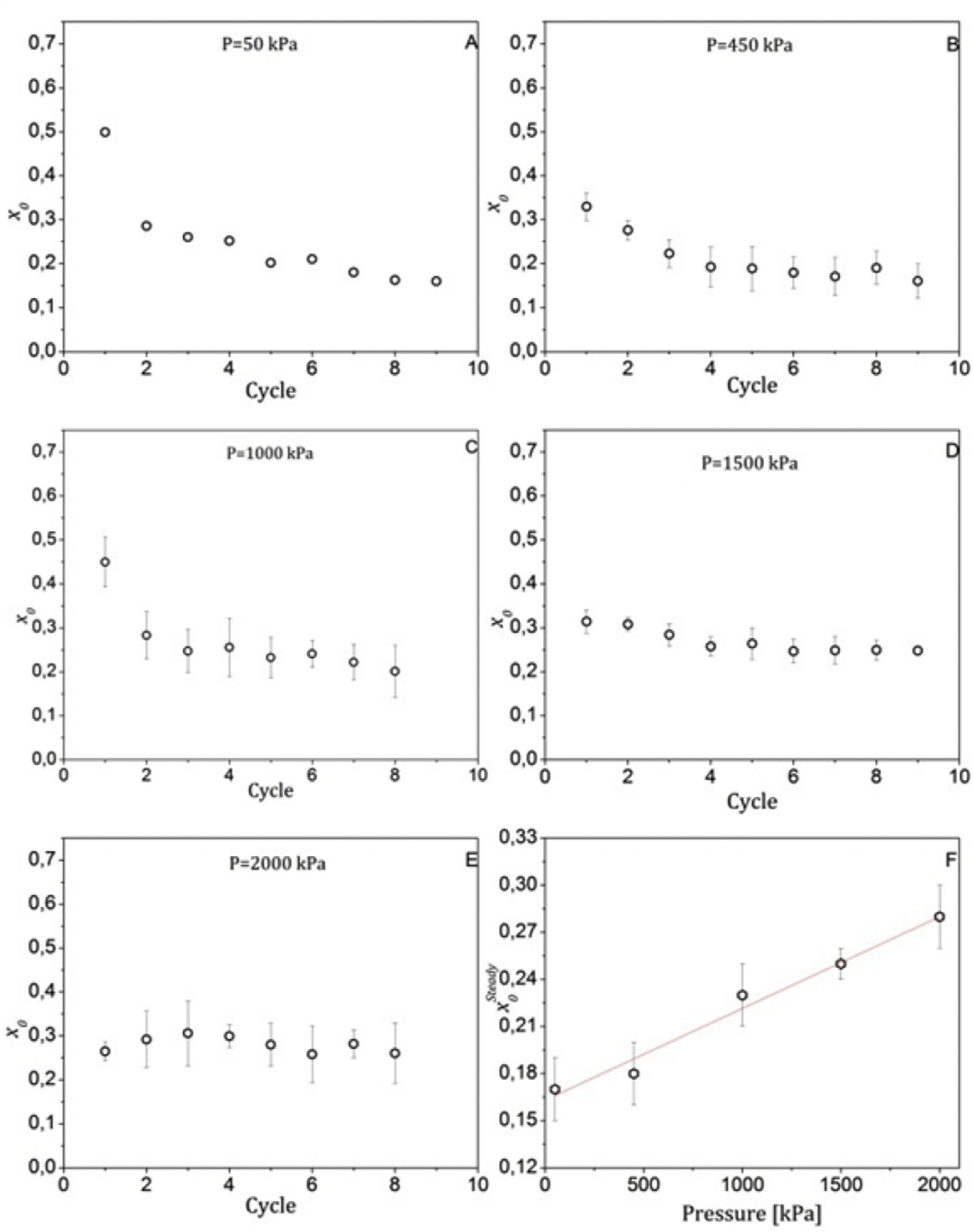

Fig. 5 – Evolution of the reacted fraction value at the controlling mechanism change (x_0) with the number of cycles for different hydrogen back pressures (A–E) and calculated x_0^{steady} for each back pressure.

The calculated curves were able to reproduce the experimental data very accurately as it can be seen in the example of the 4th cycle in Fig. 4 (the fitting corresponding to 2000 kPa is omitted since it has already been presented in Fig. 2).

Once all the measurements were adequately fitted, the values of the obtained parameters and the dependence on pressure and cycle number were analyzed in order to clarify the behavior of the system. Fig. 5A–E shows the evolution of the parameter x_0 with the number of absorption/desorption

cycles. It can be noticed that the variation of the parameter becomes less pronounced with increasing pressures. At 2000 kPa, x_0 seems to be constant within the error margin. This could be an indication that the path followed by the material at 2000 kPa is different from the one observed at lower pressures.

In order to determine the contribution of each stage to the reaction, the steady state value of x_0 was calculated as the average of the values of the last 5 cycles, since all the samples had already reached the steady state at this point. This value allows determining the behavior of the system after several hydrogen absorption/desorption cycles.

As can be seen in Fig. 5F, the (steady state) value of the parameter x_0 increases with increasing pressures, this is an indication that, at lower pressures, diffusion becomes the controlling mechanism sooner than at higher pressures. This observation is in agreement with previous works [6,17,19,20]. A possible explanation for this is that, at higher pressures, the higher amount of hydrogen molecules surrounding the material inhibits desorption on the surface. Since at the beginning of the desorption process the controlling mechanism is related to the new phase nucleation and growth, the inhibition of the reaction could make this process slower. The lower pressures may allow a higher number of possible nucleation points that can rapidly create a thin dehydrogenated shell. When this happens, the hydrogen diffusion through this shell, from the core of the material to the surface, becomes the limiting step. At higher pressures, the lower quantity of nucleation locations causes a delay in the shell formation and thus the nucleation mechanism keeps controlling the reaction up to much higher values than the reacted fraction. This evolution for low and high back pressures is schematized in Fig. 6.

The dependence of the steady state value of x_0 with back pressure was fitted with a linear model. This allows to determine the contribution of each mechanism to the desorption reaction at a given pressure. The obtained expression is the following:

$$x_0^{Steady} = 0.16 + 5.9\ 10^{-5}\ P. \quad 03$$

While understanding the desorption mechanism and its limiting steps can be useful to determine the path to follow to improve the system performance, the most important factors to analyze are the reactions kinetic constants of the two models and their evolution with the hydrogen absorption/desorption cycles.

Fig. 7 shows the evolution, with the number of cycles, of the kinetic constants (K_1 and K_2) associated with the two different kinetic equations normalized to the first cycle (K_1^1 and K_2^1 respectively). As it can be seen in the figures, at all pressures, the reaction kinetics becomes slower after the first cycle.

This effect is particularly notorious at higher pressures, where the values decrease even steeper. The kinetic constant variation with cycles was fitted with a function with the form $K = K^{steady} + Ae^{-n/\tau}$, where K^{steady} is the steady state (final) value of the kinetic constant, A is the pre-exponential factor, n is the cycle number, and τ is the factor that takes into account the amount of cycles required to reach the steady state. The analyses of some of these parameters can give information about the different phenomena occurring in the system at different pressures. The magnitude of the parameters τ and A for K_1 can be considered as indicators of the process that occur in the first dehydrogenation cycles that may lead to different pathways of hydrogen absorption/desorption at different back pressures. They also provide information about how long it takes to the system to complete the process. The obtained values of A for the desorptions at 2000 kPa ($8.4{\cdot}10^{-3}\ s^{-1}$) were one order of magnitude higher than the corresponding values for the desorptions at 50, 450 and 1000 kPa ($7.7{\cdot}10^{-4}$, $8.1{\cdot}10^{-4}$ and $9.2{\cdot}10^{-4}\ s^{-1}$ respectively), indicating that the evolution of the system is much faster at higher back pressures.

Similarly, the parameter τ is smaller for the high pressure desorptions, which relates to a faster evolution. For hydrogen storage applications, the most important parameter is the K^{steady} since it is the one that will define the desorption rate in-operando.

Fig. 8 A shows the dependence of the kinetic constant of the initial model with pressure. The values can be fitted with very good agreement to a linear model as shown in the figure. Using this linear regression, it is possible to obtain an expression for the kinetic constant of the hydrogen desorption in the first stages of the reaction:

$$K_1^{Steady} = 0.0064 - 2.63\ 10^{-6}P. \quad 04$$

with P in kPa.

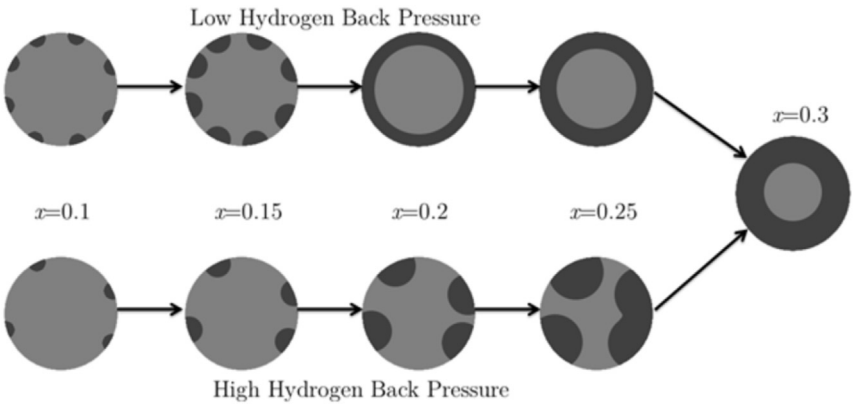

Fig. 6 – Scheme of the evolution of the dehydrogenated phase at low and high hydrogen back pressures.

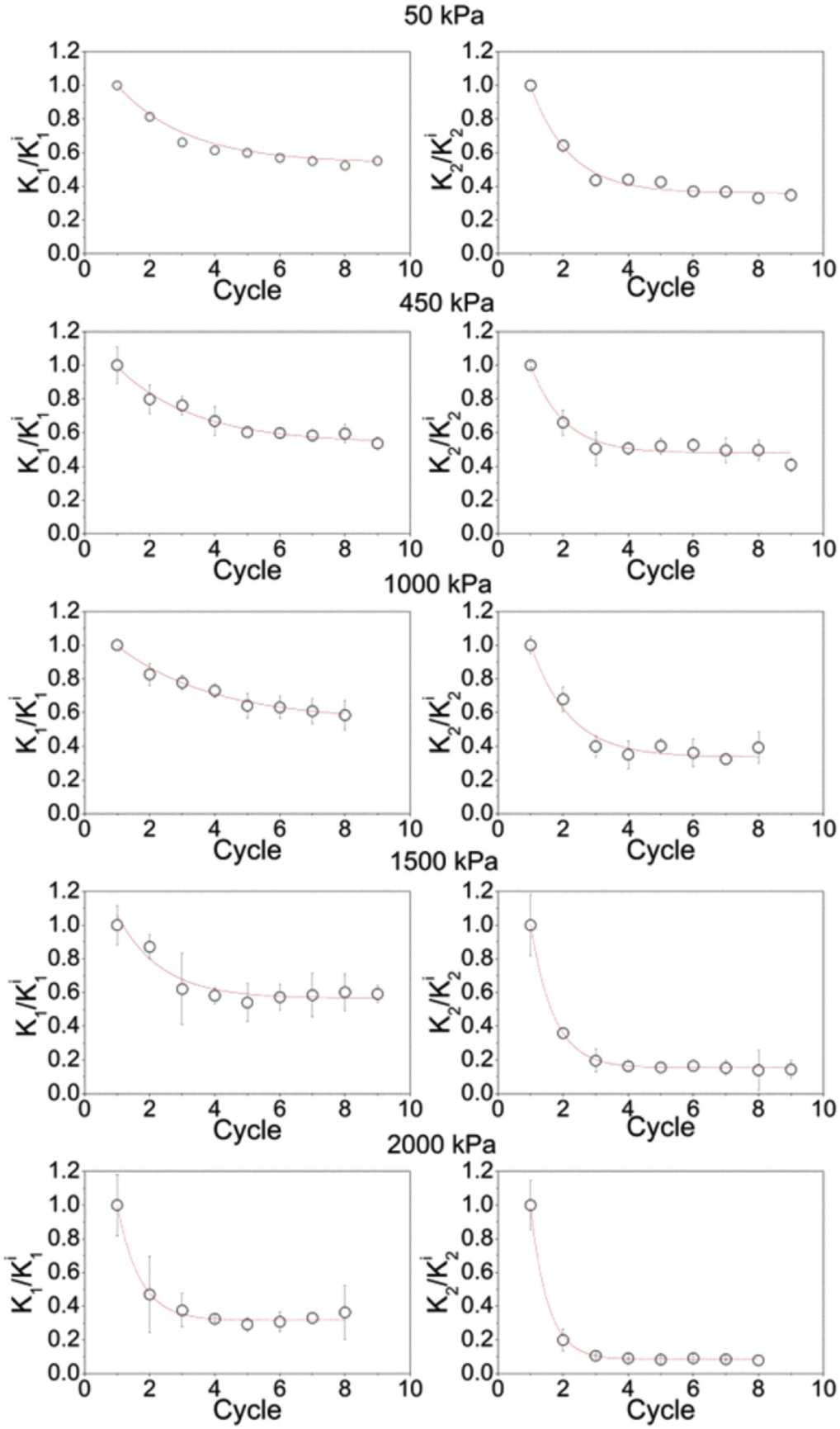

Fig. 7 – Evolution of the normalized kinetic constants K_1 and K_2 with cycling for different hydrogen back pressures.

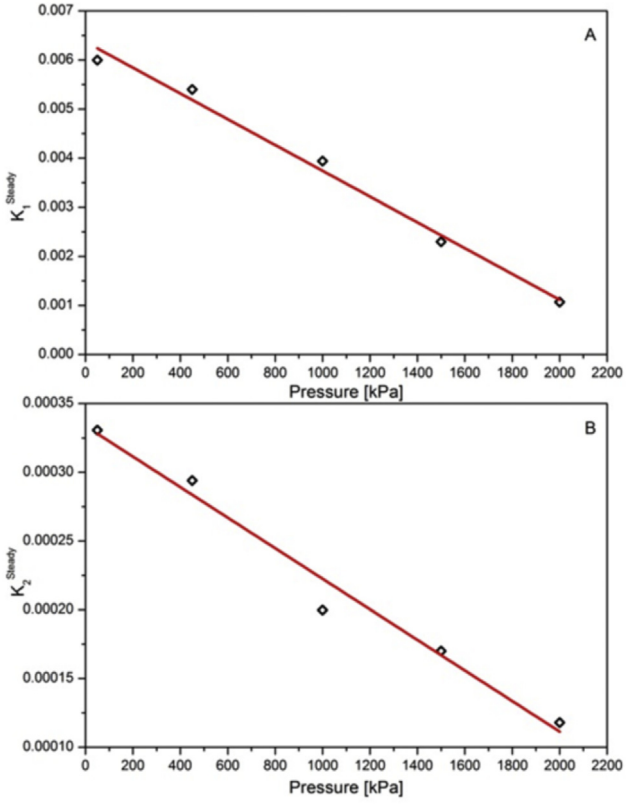

Fig. 8 – Dependence of the kinetic constant (K_1^{Steady}) of the initial Avrami mechanism (A2) (A) and (K_2^{Steady}) of the final diffusion mechanism (D3) (B) with different hydrogen back pressures.

The same analysis can be performed with the kinetic constants of the final model as shown in Fig. 8B. Again, the data was fitted to a linear model in order to obtain the dependence of the kinetic constant with pressure. In this case it is important to note that the values of K_2 are the steady state values. If the values for the first cycle are considered, the trend is reverted, with $K_2{}^1$ increasing at higher pressures. However, the most interesting values for hydrogen storage are the values obtained after several cycles, which have been presented in the figure. From the regression presented, it was possible to calculate the kinetic constant as a function of the hydrogen back pressure:

$$K_2^{Steady} = 3.3\,10^{-4} - 1.11\,10^{-7}P. \qquad 05$$

with P in kPa.

Combining equations (02A), (02B) (03), (04) and (05), it is possible to obtain an expression for the isothermal reaction rate of hydrogen desorption in the $Mg(NH_2)_2$–2LiH system with $Li_4(NH_2)_3BH_4$ as additive. In the steady state, the reaction rate can be expressed as:

$$r = \alpha_1 r_1 + \alpha_2 r_2 \qquad 01$$

with:

$$\alpha_1 = 1 - \frac{1}{1 + e^{-40(x-0.17+5.2\ 10^{-5}P)}}$$

$$\alpha_2 = \frac{1}{1 + e^{-40(x-0.17+5.2\ 10^{-5}P)}}$$

$$r_1 = 2\left(0.0064 - 2.63\ 10^{-6}P\right)(1-x)\left(-\ln(1-x)\right)^{1/2}$$

$$r_2 = \left(3.3\ 10^{-4} - 1.11\ 10^{-7}P\right)\frac{3(1-x)^{2/3}}{2\left(1-(1-x)^{1/3}\right)}$$

These equations allow the prediction of hydrogen desorption rate as a function of pressure and the reacted fraction in the $Li_4(NH_2)_3BH_4$ doped $Mg(NH_2)_2$–2LiH, which can be used for simulations of hydrogen storage tanks in real operation conditions.

Conclusions

In this work, the hydrogen desorption performance in the $Li_4(NH_2)_3BH_4$ doped $Mg(NH_2)_2$–2LiH was studied at a wide range of pressures. The evolution of the system during successive hydrogen absorption/desorption cycles was also evaluated. The dehydrogenation behavior under cycling showed a beneficial effect of $Li_4(NH_2)_3BH_4$ in the composite in the experimental conditions studied and can be associated with a catalytic effect. The changes observed in the system during the first cycles before reaching the steady state could be related to the formation of $Li_4(NH_2)_3BH_4$ from the original $LiBH_4$ initially introduced in the mixture. By proposing and fitting several model equations, it was possible to determine that a single mechanism model was not able to reproduce the behavior of the reaction at both lower and higher reaction fractions simultaneously. For this reason, a combination of two controlling mechanism models was proposed. This combined model was able to reproduce with high accuracy the behavior of the system for the pressure range studied.

The combination of controlling mechanisms that showed the best accuracy was a second grade Avrami mechanism model at lower conversions which evolved to a 3D diffusion model through the course of the dehydrogenation. Since the second grade Avrami model can be physically related to a nucleation and growth phenomenon, these results suggest that, at the beginning, the limiting step of the reaction is the formation of the products, until a thin layer of product is formed on the surface. At this transition point, the diffusion through this layer becomes the new limiting step.

This suggestion is further reinforced by the observation of the evolution of the mentioned transition point with pressure, which indicates that at high pressures the mechanism change occurs later during desorption. This could be related to the higher difficulty in creating nucleation points on a surface exposed to a higher concentration of hydrogen.

The main contribution of this work is that it enables the prediction of the system behavior. These results are crucial for the design of solid-state based hydrogen storage tanks, since the obtained final equation could be used to estimate the dehydrogenation rate as a function of the reacted fraction and

hydrogen back pressure. Moreover, this study provides interesting guidelines for improving the reaction kinetics of the system. In fact, it shows that the strategies to enhance hydrogen desorption should be addressed to not only modify the diffusion through the product layer, but also the nucleation and growth step.

Acknowledgements

This study has been partially supported by CONICET (National Council of Scientific and Technological Research), CNEA (National Commission of Atomic Energy), ANPCyT (PICT N° 1052) and Instituto Balseiro (University of Cuyo).

REFERENCES

[1] Nakamori Y, Kitahara G, Orimo S. Synthesis and dehydriding studies of Mg–N–H systems. J Power Sources 2004;138:309–12.
[2] Luo W, Rönnebro E. Towards a viable hydrogen storage system for transportation application. J Alloy Compd 2005;404–406:392–5.
[3] Luo W, Stavila V, Klebanoff LE. New insights into the mechanism of activation and hydrogen absorption of $2LiNH_2$–MgH_2. Int J Hydrogen Energy 2012;37:6646–52.
[4] Hu J, Liu Y, Wu G, Xiong Z, Chen P. Structural and compositional changes during hydrogenation/dehydrogenation of the Li–Mg–N–H system. J Phys Chem C 2007;111:18439–43.
[5] Chen Y, Wu Cheng-Zhang, Wang Ping, Cheng Hui-Ming. Structure and hydrogen storage property of ball-milled $LiNH_2$-MgH_2 mixture. Int J Hydrogen Energy 2006;31:1236–40.
[6] Liu Y, Zhong K, Luo K, Gao M, Pan H, Wang Q. Size-dependent kinetic enhancement in hydrogen absorption and desorption of the Li–Mg–N–H system. J Am Chem Soc 2009;131:1862–70.
[7] Nayebossadri S. Kinetic rate-limiting steps in dehydrogenation of Li–N–H and Li–Mg–N–H systems – effects of elemental Si and Al. Int J Hydrogen Energy 2011;36:8335–43.
[8] Liang C, Liu YF, Gao MX, Pan HG. Understanding the role of K in the significantly improved hydrogen storage properties of a KOH-doped Li–Mg–N–H system. J Mater Chem A 2013;1:5031–6.
[9] Liu YF, Li C, Li B, Gao MX, Pan HG. Metathesis reaction-induced significant improvement in hydrogen storage properties of the KF-Added Mg(NH2)2–2LiH system. J Phys Chem C 2013;117:866–75.
[10] Wang JH, Liu T, Wu GT, Li W, Liu YF, Araujo CM, et al. Potassium-modified $Mg(NH_2)_2$/2 LiH system for hydrogen storage. Angew Chem Int Ed 2009;48:5828–32.
[11] Hu JJ, Fichtner M, Chen P. Investigation on the properties of the mixture consisting of Mg(NH2)2, LiH, and $LiBH_4$ as a hydrogen storage material. Chem Mater 2008;20:7089–94.
[12] Hu JJ, Liu YF, Wu GT, Xiong ZT, Chua YS, Chen P. Improvement of Hydrogen storage properties of the Li–Mg–N–H system by addition of $LiBH_4$. Chem Mater 2008;20:4398–402.
[13] Yang J, Sudik A, Siegel DJ, Halliday D, Drews A, Carter RO, et al. A self-catalyzing hydrogen-storage material. J W Low Angew Chem Int Ed 2008;47:882–7.
[14] David WIF. A mechanism for non-stoichiometry in the lithium amide/lithium imide hydrogen storage reaction. J Am Chem Soc 2007;129:1594–601.
[15] Wu H. Structure of ternary imide $Li_2Ca(NH)_2$ and hydrogen storage mechanisms in amide–hydride system. J Am Chem Soc 2008;130:6515–22.
[16] Chen P, Xiong ZT, Yang LF, Wu GT, Luo WF. Mechanistic investigations on the heterogeneous solid-state reaction of magnesium amides and lithium hydrides. J Phys Chem B 2006;110:14221–5.
[17] Markmaitree T, Shaw LL. Synthesis and hydriding properties of $Li_2Mg(NH)_2$. J Power Sources 2010;195:1984–91.
[18] Liang C, Gao M, Pan H, Liu Y, Yan M. Effect of gas back pressure on hydrogen storage properties and crystal structures of $Li_2Mg(NH)_2$. Int J Hydrogen Energy 2014;39:17754–64.
[19] Hayes J, Goudy A. Thermodynamics, kinetics and modeling studies of KH- RbH- and CsH-doped $2LiNH_2$/MgH_2 hydrogen storage systems. Int J Hydrogen Energy 2015;40:12336–42.
[20] Durojaiye T, Hayes J, Goudy A. Potassium, rubidium and cesium hydrides as dehydrogenation catalysts for the lithium amide/magnesium hydride system. Int J Hydrogen Energy 2015;40:2266–73.
[21] Cao HJ, Wu GT, Zhang Y, Xiong ZT, Qiu JS, Chen P. Effective thermodynamic alteration to $Mg(NH_2)_2$–LiH system: achieving near ambient-temperature hydrogen storage. J Mater Chem A 2014;2:15816–22.
[22] Anderson PA, Chater PA, Hewett DR, Slater PR. Hydrogen storage and ionic mobility in amide–halide systems. Faraday Discuss 2011;151:271–84.
[23] Amica G, Cova F, Arneodo Larochette P, Gennari FC. Effective participation of $Li_4(NH_2)_3BH_4$ in the dehydrogenation pathway of the $Mg(NH_2)_2$–2LiH composite. Phys Chem Chem Phys 2016;18:17997–8005.
[24] Khawam A, Flanagan D. Role of isoconversional methods in varying activation energies of solid-state kinetics I. isothermal kinetic studies. Thermochim Acta 2005;429:93–102.
[25] Eiben AE. Evolutionary computing. Inf Process Lett 2002;82:1–6.
[26] Cova F, Gennari F, Arneodo Larochette P. Numerical modeling of hydrogen absorption measurements in Ni-catalyzed Mg. Int J Hydrogen Energy 2014;39:5010–8.
[27] Cova F, Gennari F, Arneodo Larochette P. Hydrogen absorption in Ni-catalyzed Mg: a model for measurements in the low temperature range. Int J Hydrogen Energy 2014;39:11501–8.
[28] Pang Y, Li Q. A review on kinetic models and corresponding analysis methods for hydrogen storage materials. Int J Hydrogen Energy 2016:1–16.
[29] Lozano GA, Ranong CN, Bellosta von Colbe JM, Bormann R, Fieg G, Hapke J, et al. Empirical kinetic model of sodium alanate reacting system (II). Hydrogen desorption. Int J Hydrogen Energy 2010;35:7539–46.